Electronic Supplementary Information

Low-Frequency Noise in Multilayer MoS_2 Field-Effect Transistors: The Effect of High-k Passivation

Junhong Na,[a] Min-Kyu Joo,[a,b] Minju Shin,[a,b] Junghwan Huh,[c] Jae-Sung Kim,[a] Mingxing Piao,[a] Jun-Eon Jin,[a] Ho-Kyun Jang,[a] Hyung Jong Choi,[d] Joon Hyung Shim[d] and Gyu-Tae Kim*[a]

[a]*School of Electrical Engineering, Korea University, Seoul 136-713, South Korea. E-mali: gtkim@korea.ac.kr*
[b]*IMEP-LAHC, Grenoble INP-MINATEC, 3 Parvis Louis Neel, 38016 Grenoble, France*
[c]*Department of Electronics and Telecommunications, Norwegian University of Science and Technology, NO-7491 Trondheim, Norway*
[d]*School of Mechanical Engineering, Korea University, Seoul 136-713, South Korea*

Minimizing the contact resistance change by thermal annealing

The effects of high-k dielectrics on MoS_2 FETs have been discussed in terms of material properties extracted from the device characteristics, such as the field-effect mobility.[1-3] However, it is not straightforward to determine the relationships between a high-k dielectric and μ_{FE} because the calculation of μ_{FE} does not take into account changes in the contact resistance.[2, 3] During the ALD process used to deposit the Al_2O_3 on the multilayer MoS_2 film, the growth temperature may cause thermal annealing, which can affect the device characteristics, and in particular may significantly influence the contact resistance. To ensure that the deposition of the Al_2O_3 layer did not cause spurious changes in the device characteristics resulting from the temperature profile during the ALD process, the same thermal profile was applied to devices where Al_2O_3 was not grown by placing the structures in the reactor, and the growth precursors were not injected. The conditions in the reactor were ~ 7×10^{-2} Torr and 220°C, and the total process time was 10 hours. Before this thermal annealing process, the as-fabricated multilayer MoS_2 FETs exhibited Schottky contact behavior, as can be seen from the characteristics shown in Fig S1. After thermal annealing, however, the current in the multilayer MoS_2

transistor significantly increased and the device characteristics were consistent with Ohmic contact behavior.

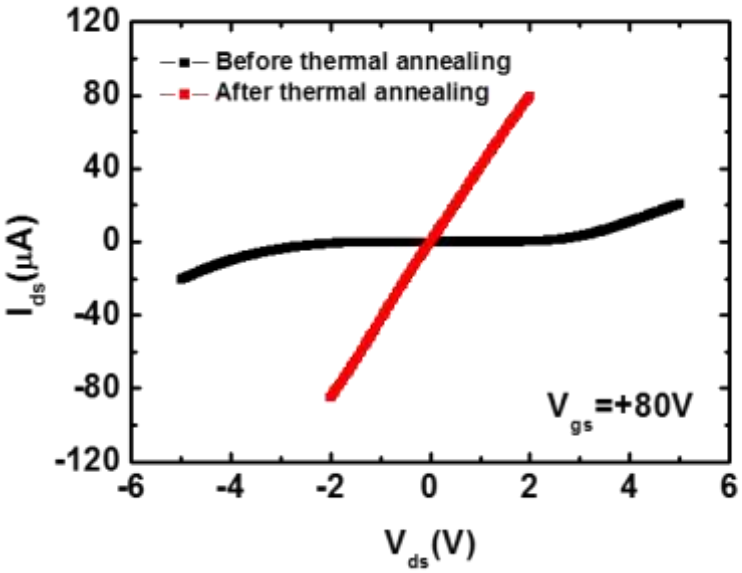

Fig S1. Output characteristics of the multilayer MoS_2 FET at a gate voltage of V_{gs} = 80 V before and after the thermal annealing process.

Off-current increase phenomena due to the Al_2O_3 passivation

Fig S2(a) showed the change of the on current and the off-current in the several multilayer MoS_2 FETs after the Al_2O_3 passivation. All devices that we measured showed two or three orders of magnitude increase of the off-current after the Al_2O_3 passivation. Due to the increase of the off-current, the on/off ratio was decreased as expressed in Fig S2(b). All these devices were thermally annealed before the Al_2O_3 passivation as mentioned earlier.

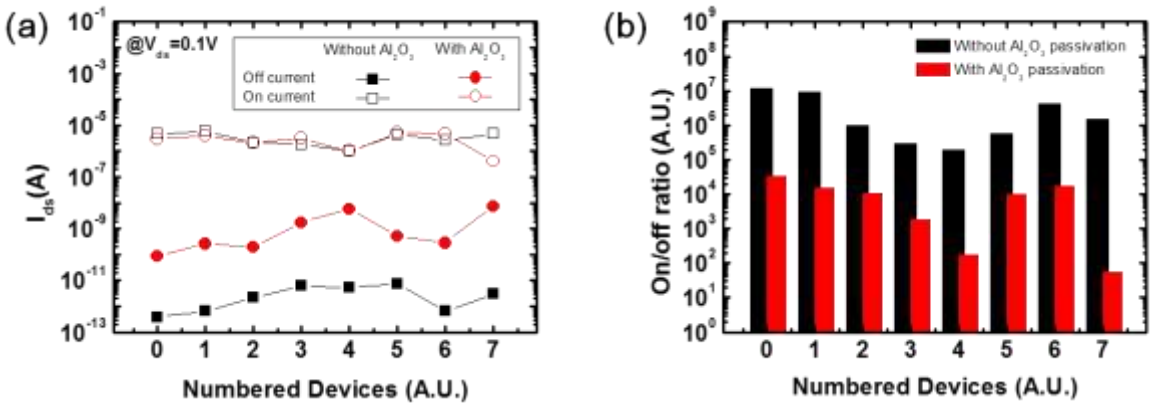

Fig S2. (a) On current, off-current, (b) and on/off ratio of the several multilayer MoS_2 FETs without and with the Al_2O_3 passivation.

Three-dimensional numerical simulations to calculate the gate capacitance

When extracting the field-effect mobilities from measurements of devices fabricated using 2-D materials – such as the graphene and the MoS_2 FETs reported here – the gate capacitance is often calculated assuming a parallel-plate capacitor model.[4-6] However, more accurate calculations of the gate capacitance with increased accuracy in the determination of μ_{FE} should account for the gate fringing field and the dielectric constant of the passivation layer.[7]

In order to compare the devices with and without the Al_2O_3 passivation layer, numerical simulations were carried out using COMSOL Multiphysics v4.3a. Fig S3(a) and (b) show cross-sectional schematic images of the simulated geometries of the devices with and without the Al_2O_3 passivation layer.

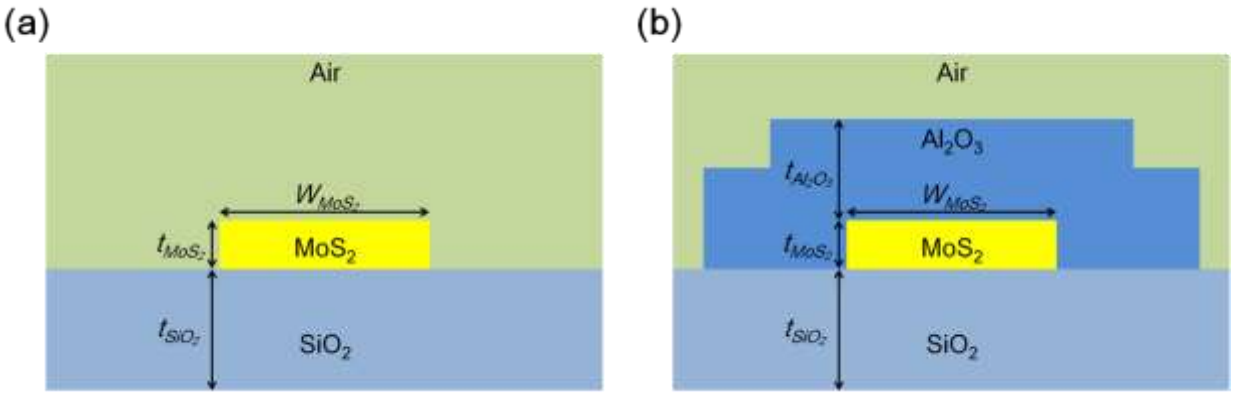

Fig S3. Cross-sectional schematic images of the multilayer MoS_2 FETs (a) without and (b) with the Al_2O_3 passivation. The channel width was W_{MoS2} = 2.3 μm and the channel length was L_{MoS2} = 0.28 μm. The thickness of the MoS_2 layer was t_{MoS2} = 11.3 nm, the thickness of the Al_2O_3 layer was t_{Al2O3} = 30 nm, and the thickness of the SiO_2 layer was t_{SiO2} = 300 nm.

Fig S4(a) shows the three-dimensional (3-D) geometries that were used in the numerical simulations with the Al_2O_3 passivation layer. The electric potential (V) can be numerically calculated in the all over the region which is designed in the geometry of the simulation by solving the Poisson equation for electrostatics:

$$\nabla^2 V = -\frac{\rho}{\varepsilon_0 \varepsilon_r} \quad \text{(S1)}$$

where ε_0 and ε_r are vacuum permittivity and relative permittivity, respectively, ρ is the charge density. According to the relation between V and electric field (E), the E can be also obtained:

$$E = -\nabla V \quad \text{(S2)}$$

Fig S4(b) and c show simulated electric potential distributions. According to the relation between the capacitance (C) and the energy for charging a capacitor (W_e), the capacitance can be calculated:

$$C = -\frac{Q^2}{2W_e} \quad \text{(S3)}$$

where Q is the total charge. The W_e can be expressed as:

$$W_e = \int_{\Omega} (\varepsilon_0 \varepsilon_r E \cdot E) dV \tag{S4}$$

By following the above process, the calculated gate capacitance was 1.87×10^{-16} F without Al_2O_3 passivation and 2.23×10^{-16} F with Al_2O_3 passivation. The difference between these two capacitances is 19.2%.

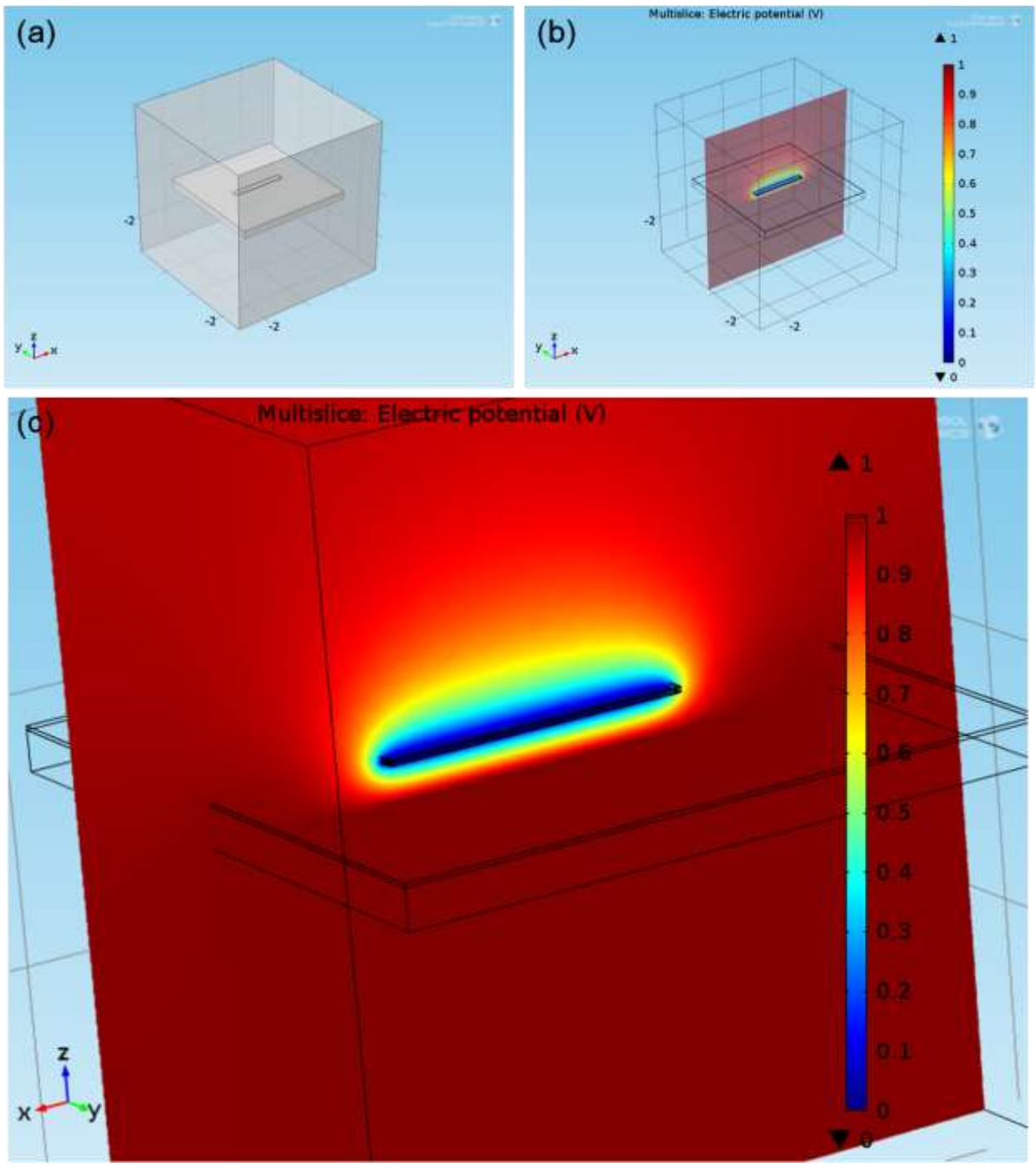

Fig S4. Simulated data from the 3-D electrostatics calculations of the device with the Al_2O_3 passivation layer. (a) Geometry of the multilayer MoS_2 FET. (b) Electric potential distribution in a 2-D plane and (c) a close-up of these data.

Raw LFN data

The raw data used to calculate the LFN spectra for the multilayer MoS_2 FETs are shown in Fig S5(a) (without) and Fig S5(b) (with) the Al_2O_3 layer. All of these noise data exhibit a 1/*f* dependence at all gate voltages. Due to the measurement limit of the noise spectral density, S_I (which was ~ 10^{-25} A^2Hz^{-1}), some data do not appear to follow the 1/*f* dependence. However, data in the range 10–20 Hz did follow the 1/*f* dependence. Therefore, we used data that lay within this frequency range.

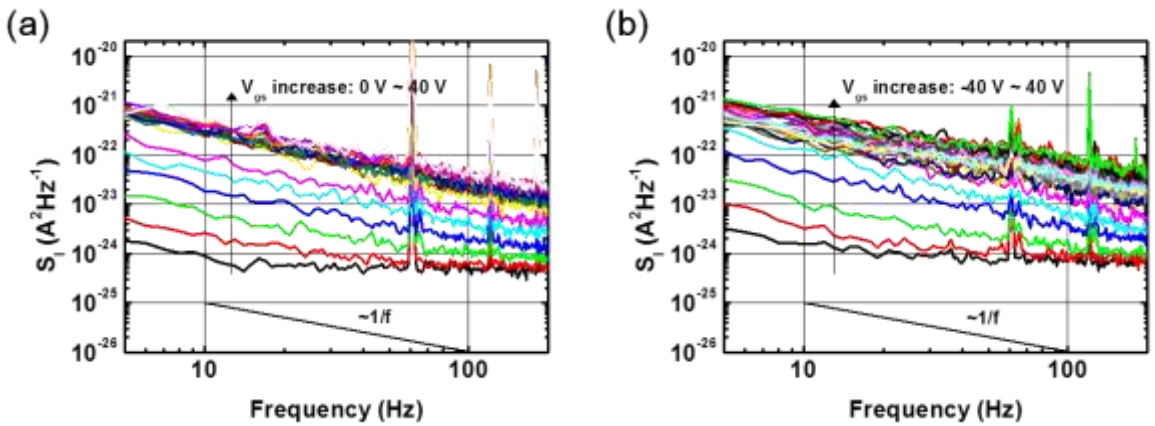

Fig S5. Noise spectral density, S_I, as a function of frequency (a) without and (b) with the Al_2O_3 passivation layer at a range of gate voltages. 60-Hz noise and harmonics thereof are visible in the data.

In order to make sure that the low-frequency noise of the multilayer MoS_2 FETs follows the 1/f dependence, we extracted the frequency exponent (γ) by fitting the data to the Hooge's empirical equation:

$$\frac{S_I}{I_{ds}^{\ 2}} = \frac{\alpha_H}{Nf^{\gamma}} \tag{S5}$$

where α_H is the Hooge parameter, N is the total number of charge carriers, f is the frequency. The extracted γ values were in the range from ~ 0.9 to ~ 1.1 for both without and with Al_2O_3 passivation, which were close to the unity.

The drain current exponent (β) values can be extracted by fitting the data to the HMF equation :

$$S_I = \frac{q\alpha_H \mu V_{ds}}{fL^2} \cdot I_{ds} \tag{S6}$$

which is the same equation (4) in the main text. According to the equation (S6), the S_I value can be proportional to the I_{ds} (β ~1) in the HMF dominant region. In the Fig S6(a), the β values were extracted as ~ 1.08 and ~ 0.91 without and with Al_2O_3, respectively. The regions that were selected for the fittings are that the HMF models are dominant in the noise properties for both without and with Al_2O_3.

Fig S6(b) shows the Hooge parameter (α_H) versus the drain current without and with Al_2O_3. Basically, the α_H values is more reasonable to the HMF model, so the meaningful values of α_H are likely to placed in the HMF dominant regime. In the main text, the α_H values for both without and with Al_2O_3 were obtained as ~ 2.5×10^{-3}. This value is very similar with the values in the HMF dominant regime for both without and with Al_2O_3.

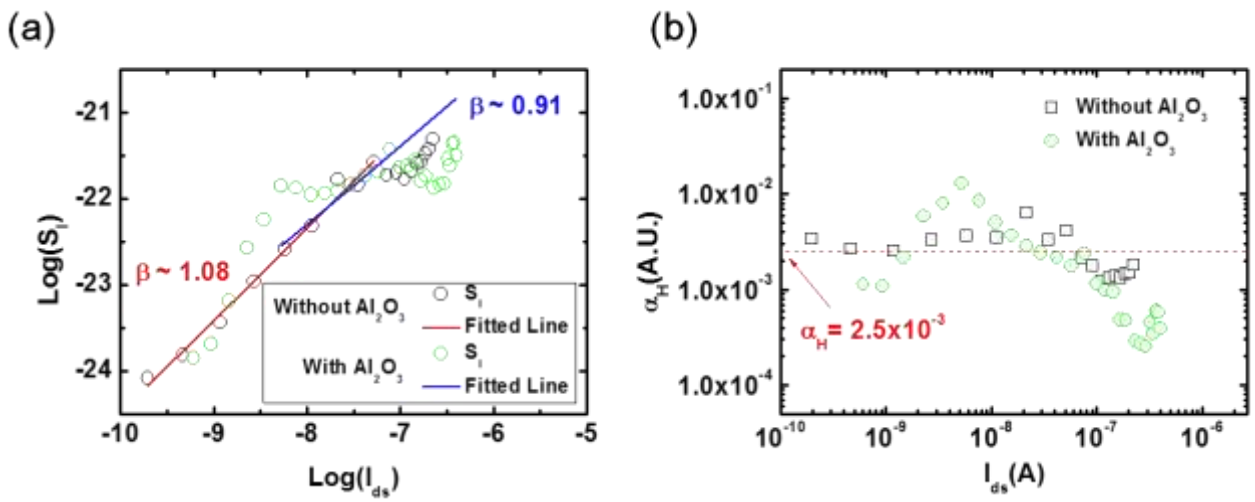

Fig S6. (a) The spectral density as a function of the drain current plotted in log scale is shown without and with the Al_2O_3 passivation layer. (b) Hooge parameter as a function of the drain current without and with the Al_2O_3 passivation layer.

Energy band diagrams

Energy band diagrams for each material are shown in Fig S7. The work function of titanium of 4.3 eV was used as the gate metal work function. The electron affinity of MoS_2 was 4.0 eV and the band gap was 1.2 eV.[4, 8]

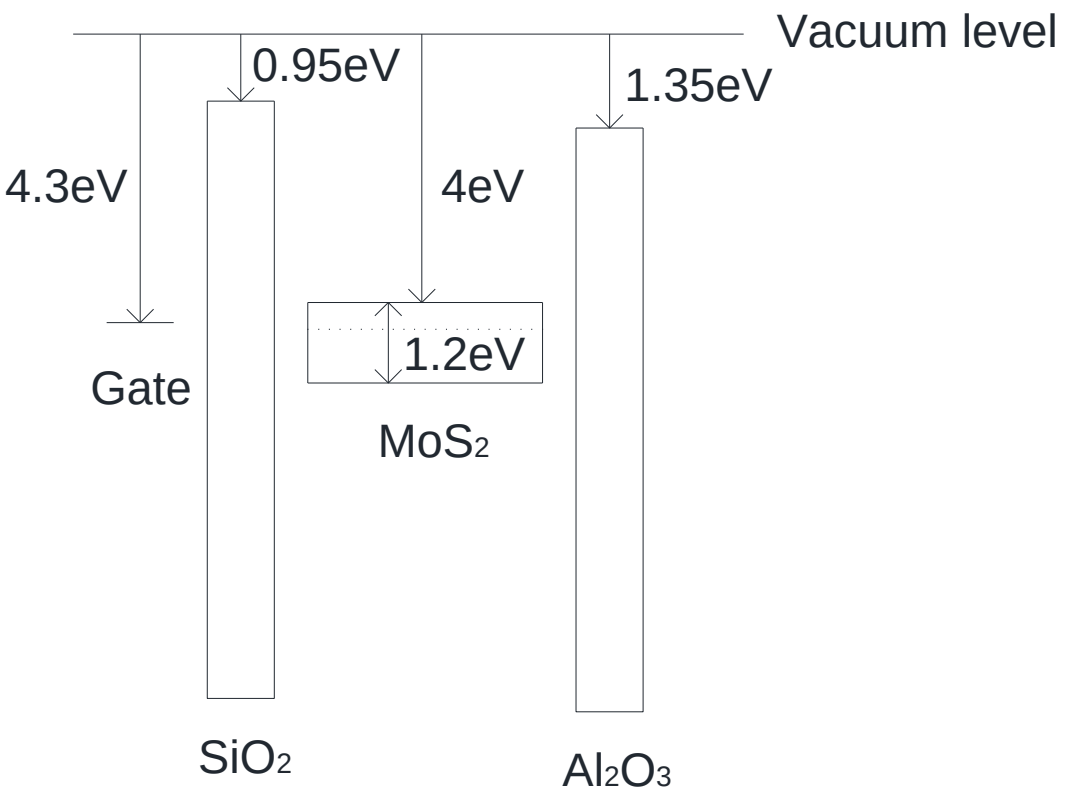

Fig S7. Energy band diagram of the MoS_2 FET with the Al_2O_3 passivation layer.

References

1. B. Radisavljevic, A. Radenovic, J. Brivio, V. Giacometti and A. Kis, *Nat Nano*, 2011, **6**, 147-150.
2. M. S. Fuhrer and J. Hone, *Nat Nano*, 2013, **8**, 146-147.
3. B. Radisavljevic and A. Kis, *Nat Nano*, 2013, **8**, 147-148.
4. S. Das, H.-Y. Chen, A. V. Penumatcha and J. Appenzeller, *Nano Lett.*, 2012, **13**, 100-105.
5. S. Kim, A. Konar, W. S. Hwang, J. H. Lee, J. Lee, J. Yang, C. Jung, H. Kim, J. B. Yoo, J. Y. Choi, Y. W. Jin, S. Y. Lee, D. Jena, W. Choi and K. Kim, *Nat. Commun.*, 2012, **3**, 1011.
6. H. Qiu, L. Pan, Z. Yao, J. Li, Y. Shi and X. Wang, *Appl. Phys. Lett.*, 2012, **100**, 123104.
7. O. Wunnicke, *Appl. Phys. Lett.*, 2006, **89**, 083102-083103.
8. S. W. Han, H. Kwon, S. K. Kim, S. Ryu, W. S. Yun, D. H. Kim, J. H. Hwang, J. S. Kang, J. Baik, H. J. Shin and S. C. Hong, *Physical Review B*, 2011, **84**, 045409.